Research in Astron. Astrophys. **2012** Vol. **12** No. **11**, 1585–1596
http://www.raa-journal.org *http://www.iop.org/journals/raa*

***R**esearch in*
***A**stronomy and*
***A**strophysics*

The photometric system of the Tsinghua-NAOC 80-cm telescope at NAOC Xinglong Observatory *

Fang Huang[1,2], Jun-Zheng Li[2], Xiao-Feng Wang[2], Ren-Cheng Shang[2],
Tian-Meng Zhang[3,4], Jing-Yao Hu[3], Yu-Lei Qiu[3] and Xiao-Jun Jiang[3,4]

[1] Astronomy Department, Beijing Normal University, Beijing 100875, China; *hfbnu111@gmail.com*
[2] Physics Department and Tsinghua Center for Astrophysics, Tsinghua University, Beijing 100084, China;
[3] National Astronomical Observatories, Chinese Academy of Sciences, Beijing 100012, China;
[4] Key Laboratory of Optical Astronomy, National Astronomical Observatories, Chinese Academy of Sciences, Beijing 100012, China

Received 2012 March 5; accepted 2012 May 29

Abstract The Tsinghua-NAOC (National Astronomical Observatories of China) Telescope (hereafter, TNT) is an 80-cm Cassegrain reflecting telescope located at the Xinglong Observatory of NAOC, with the main scientific goals of monitoring various transients in the universe such as supernovae, gamma-ray bursts, novae, variable stars, and active galactic nuclei. We present a systematic test and analysis of the photometric performance of this telescope. Based on the calibration observations taken on 12 photometric nights, spanning the period from 2004 to 2012, we derived an accurate transformation equation between the instrumental $ubvri$ magnitudes and standard Johnson UBV and Cousins RI magnitudes. In particular, the color terms and the extinction coefficients of different passbands are well determined. With these data, we also obtained the limiting magnitudes and the photometric precision of TNT. It is worthwhile to point out that the sky background at the Xinglong Observatory became gradually worse over the period from 2005 to 2012 (e.g., ∼21.4 mag vs. ∼20.1 mag in the V band).

Key words: instrumentation: detectors — site testing — telescopes

1 INTRODUCTION

The Tsinghua-National Astronomical Observatories of China (NAOC) Telescope (TNT), the first professional telescope owned by a university in China, is an 80-cm Cassegrain telescope made by APM-Telescopes[1] in Germany. This telescope is located at the Xinglong Observing Station of NAOC ($117°34'39''$E, $40°23'40''$N, at an elevation of ∼830 m), jointly operated by Tsinghua University and NAO, Chinese Academy of Sciences, since 2004. The main science projects conducted using TNT in recent years have been multi-color, photometric studies of supernovae (SNe, Wang et al. 2008, 2009; Wang et al. 2012 in preparation; Zhang et al. 2010; Zhang et al. 2012), active

∗ Supported by the National Natural Science Foundation of China.
[1] *http://www.apm-telescopes.com*

galactic nuclei (AGN, Liu et al. 2010; Zhai et al. 2011; Zhai & Wei 2012), and gamma-ray bursts (GRBs, Xin et al. 2010, 2011). Other projects involving this telescope include photometric observations of binary stars (Li et al. 2009; Yang et al. 2010; Yan et al. 2012; Fang et al. 2012) and variable stars (Wu et al. 2005, 2006; Fu et al. 2009). However, an overall examination of the performance of the CCD photometric system on TNT is still absent.

Knowing the properties and performance of a telescope, such as its throughput, detection limit, and instrument response, will be of great assistance to the observers in preparing their observation proposals. These parameters allow a better estimate of the exposure time and prediction of photometric precision for individual objects. We started a program to investigate the characteristics of the CCD photometric system on TNT. Relevant evaluations of the photometric system of the BATC 60/90-cm Schmidt telescope and the 85-cm telescope at the Xinglong Observatory of the NAOC are available from Yan et al. (2000) and Zhou et al. (2009), which help users better understand the performance of these facilities and work out a reasonable observing plan.

This paper is organized as follows: in Section 2, we briefly describe the TNT observation system. Then we present the CCD detector test results in Section 3. The photometric calibration results are given in Section 4. The systematic performance of TNT is addressed in Section 5, and we provide a summary in Section 6.

2 OBSERVATION SYSTEM

TNT is an f/10 'classical' Cassegrain, equatorial reflector. It has a parabolic primary mirror with an effective diameter of 0.80 m, and a hyperbolic secondary mirror with an effective diameter of 0.26 m. The pointing of the TNT is relatively fast and accurate, with maximal slew speed being up to 4° per second. At latitudes larger than $25°$, the pointing accuracy is better than $30''$. The pointing drift without guide star tracking is less than $1''$ in 15 min. The main parameters of TNT are very similar to those of the Lulin One-meter Telescope (LOT; Kinoshita et al. 2005), except for differences in the aperture of the main mirror and the cooling mode of the CCD detector.

The CCD detector mounted on TNT was made by Princeton Instruments VersArray: 1300B[2]. This is a high-performance, full-frame digital camera system that utilizes a back-illuminated, scientific-grade CCD. With a 1340×1300 imaging array (20×20 μm pixel^{-1}), this system provides a field-of-view (FOV) of $11.5' \times 11.2'$ with a spatial resolution of $\sim 0.52''$ pixel^{-1}.

Table 1 Parameters of the VersArray: 1300B

Features	Specifications
Pixel number	1340×1300
Pixel size	20μm×20μm
Imaging area	26.8mm×26mm
Fill factor	100%
A/D conversion	16 bits
Scan rates	100 kHz, 1 MHz
Full frame readout time	18s@100 kHz, 1.8s@1 MHz
Readout noise	2.8e$^-$@100 kHz, 8e$^-$@1 MHz
Software-selectable gains	1/2×, 1×, 2×
Dark current	0.5−1e$^-$ pix^{-1} hr^{-1}
Nonlinearity	$\leq$ 2%
Cooling medium	Liquid nitrogen
Operating temperature	−110°C
Thermostating precision	±0.05°C

The main parameters of the VersArray: 1300B CCD are listed in Table 1. It has two readout modes, with the readout time being about 18 seconds in the slow mode (100 kHz) and about 2

[2] *http://www.princetoninstruments.com*

seconds in the fast mode (1 MHz). There have been nominally three 1300B CCDs that have been used on TNT since the start of observations in 2004. The 1300B-1 CCD had been used before 2006, and later replaced by the 1300B-2 CCD during the period from 5 Jan. to 14 Jun. in 2006 for maintenance. After that, the 1300B-3 CCD was used until Sept. 2010, when it was broken, and the 1300B-1 was installed again on TNT as a replacement.

The filters used on TNT are manufactured by Custom Scientific, Inc. (USA)[3]. They are the standard Johnson UBV and Cousins RI system (Bessell 1990). This has been indicated by a small color-term correction needed to transform the photometric results from the instrumental system of TNT to the standard $UBVRI$ system (e.g., Wang et al. 2008, 2009).

3 CCD TESTS

3.1 Bias Level

A bias level is present in every CCD image, arising from an electronic offset which is added to the signal of the CCD before being converted to the digital values. Its stability has a non-negligible effect on high precision photometry. The bias level has been measured for all the three CCDs used on TNT in both the slow and fast readout modes. We performed a continuous 30-hour test of the bias for the 1300B-1 CCD, an 8-hour test for the 1300B-2, and a 7-hour test for the 1300B-3. These results are reported in Table 2.

Table 2 Bias, gain, and readout noise determined for the VersArray: 1300B CCD attached to TNT. Two readout rates at 100 kHz and 1 MHz are indicated in the brackets of Col. (2).

	Readout Mode	1300B-1 (before 2006.1)	1300B-2 (2006.1-6)	1300B-3 (after 2006.6)
Bias (ADU)	Slow Mode (100 kHz)	195±3	110±2	185±2
	Fast Mode (1 MHz)	403±6	182±4	213±5
Readout noise (e^-)	Slow Mode (100 kHz)	2.75±0.03	2.90±0.05	2.50±0.21
(findgain in IRAF)	Fast Mode (1 MHz)	9.31±0.34	5.63±0.08	5.94±0.33
Readout noise (e^-)	Slow Mode (100 kHz)	2.72±0.18	2.92±3.90	—
(fit Signal & Noise)	Fast Mode (1 MHz)	9.56±0.50	6.16±3.79	—
Gain (e^-/ ADU)	Slow Mode (100 kHz)	1.96±0.02	1.90±0.03	1.73±0.09
(findgain in IRAF)	Fast Mode (1 MHz)	2.22±0.05	1.99±0.03	1.81±0.07
Gain (e^-/ ADU)	Slow Mode (100 kHz)	1.99±0.01	1.86±0.02	—
(fit Signal & Noise)	Fast Mode (1 MHz)	2.23±0.01	1.99±0.01	—

One can see from Figure 1 that the mean bias level is related to the readout mode of the CCD. For the 1300B-1 CCD, this value is about 195 Analog-to-Digital Units (ADU) for the slow mode and about 400 ADU for the fast mode. We note that the bias measured in the fast readout mode shows some fluctuations, which might be affected by ambient factors such as the temperature. Further studies are needed to clarify this phenomenon. Owing to an instability of the bias level seen in the fast readout mode, observers are suggested to take frequent bias frames during observations to achieve high precision photometry when this mode is used.

3.2 Gain and Readout Noise

The gain (G) of a CCD is the ratio between the number of electrons recorded by the CCD chip and the counts of ADU contained in the CCD image. It is useful to know this value in order to evaluate

[3] *http://www.customscientific.com/astroresearch.html*

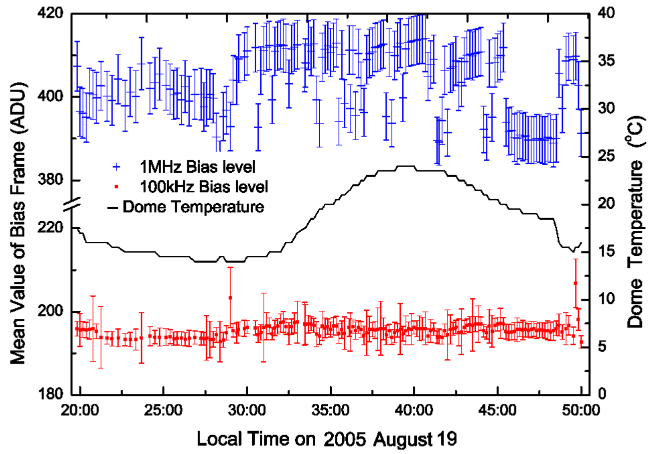

Fig. 1 The mean bias level of VersArray: 1300B-1 CCD derived in the slow and fast readout modes during a continuous 30 hour period. The solid curve represents the dome temperature during the measurements of the bias.

the performance of the CCD camera. Knowledge of the gain allows the calculation of the readout noise (R) and other quantities of the CCD. One can measure the gain of a CCD by comparing the signal level to the amount of variation in the signal, e.g., in the flatfield images. This works because the relationship between counts and electrons is different for the signal and the variance. The gain of a CCD can be determined from the following equation (Howell 2000)

$$G = \frac{(\overline{F1} + \overline{F2}) - (\overline{B1} + \overline{B2})}{\sigma^2_{F1-F2} - \sigma^2_{B1-B2}}, \tag{1}$$

where $\overline{F1}$ and $\overline{F2}$ are the mean values of different flatfield images, and $\overline{B1}$ and $\overline{B2}$ represent those of the bias images. σ^2_{F1-F2} and σ^2_{B1-B2} are the standard deviations of the difference between two flatfield images and two bias images, respectively. Subtracting two flatfield images increases the noise by a factor of $\sqrt{2}$. Therefore, the correlation between the signal S and the noise N can be expressed as

$$N = \sqrt{\frac{S}{G} + \left(\frac{R}{G}\right)^2}, \tag{2}$$

where R is the readout noise.

We took twilight flatfield images in the B band, with the exposure time varying from 0.1 s to 400 s. At each time of exposure, we took four flatfield images in the slow readout mode and another four images in the fast readout mode. We then chose two better ones and performed the subtraction to determine the standard deviation σ_F. The noise level can be obtained by dividing the standard deviation by $\sqrt{2}$. To obtain a mean signal, we subtracted the combined bias frame from the flatfield images. The noise N and signal S measured from the flatfield images are used to determine the gain and readout noise through a best fit to the relation shown by Equation (2). We also calculated these two parameters using the task FINDGAIN in IRAF[4]. Table 2 also lists the resultant gain and the readout noise derived for 1300B-1, 2, and 3 CCDs used on TNT.

[4] IRAF, the Image Reduction and Analysis Facility, is distributed by the National Optical Astronomy Observatory, which is operated by the Association of Universities for Research in Astronomy, Inc. (AURA) under cooperative agreement with the National Science Foundation (NSF).

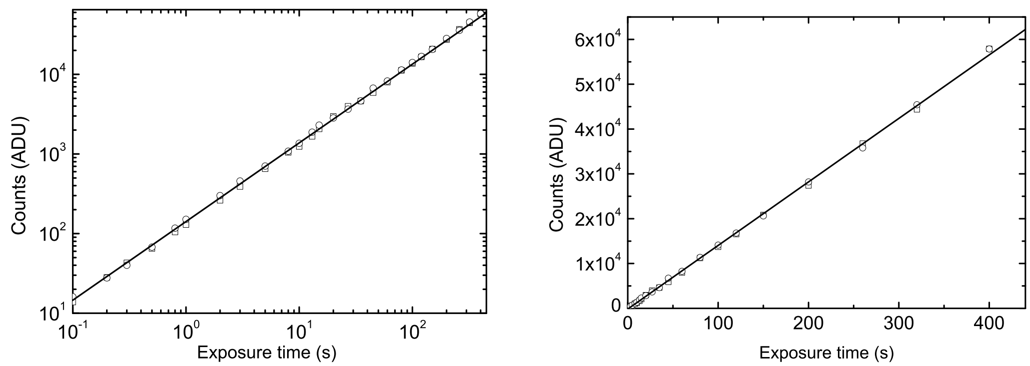

Fig. 2 ADU counts of the pixels in the flatfield images as a function of the exposure time for the 1300B-1 (*left panel*) and 1300B-2 (*right panel*). The counts in the fast mode are shown as squares and those recorded in the slow mode are denoted by circles. The straight lines show linear relationships in both modes.

3.3 Linearity of the CCD Response

One advantage of a modern CCD is its linear response over a large dynamic range. Some pixel values in the images may be unusable if they are saturated (due to the charge exceeding the full well capacity) or are within the nonlinear range. To check the linear response of the VersArray: 1300B CCD, we measured the ADU counts as a function of exposure time using the unfiltered flatfield images. For the 1300B-1 CCD, we use images taken on 2005 August 21 with exposure times of 3∼80 s, and for 1300B-2 images taken on 2006 April 6 with exposure times of 0.1∼400 s.

Figure 2 shows a relationship in both the fast and slow modes for the 1300B-1 and the 1300B-2 CCDs. One can see that the linear correlation holds for the pixel value up to ∼50 000 ADU, with the correlation coefficients of the two relations of 0.9998 and 0.9997 respectively.

3.4 Dark Current

A routine step of processing CCD images involves a subtraction of dark current. Dark current of a CCD usually originates from the collection of electrons within the potential well of a pixel in the image, which can become part of the signal and are indistinguishable from the astronomical photons. It is usually specified as the number of thermal electrons generated per second per pixel or as the actual current generated per area of the device. The thermal dark current depends on the CCD operation temperature (see fig. 3.6 in Howell 2000 for a relation between the dark current and the temperature), which becomes nearly negligible for a properly cooled CCD.

Dark frames with different integration times (e.g., 600 s and 3600 s) were obtained for the 1300B-1 CCD to estimate the dark current. We found that the mean rate of dark current generation for the 1300B-1 is about 0.00025 $\mathrm{e^{-}s^{-1}pixel^{-1}}$ for an operational temperature of -120°C. It is not surprising that the dark current level of the CCD on TNT is much lower than that of the CCD on LOT (i.e., 0.064$\mathrm{e^{-}s^{-1}pixel^{-1}}$) since the working temperature of the latter is much higher with $T = -50$°C. With the above dark current generation rate, we estimate that an observation with an exposure time of 600 s will produce a dark current of 0.15$\mathrm{e^{-}pixel^{-1}}$. This is far less than the signal and noise. Hence, we neglect such a minor effect in our image reduction.

4 PHOTOMETRIC CALIBRATIONS

The magnitudes obtained by TNT are the instrumental magnitudes. To compare our photometric results with those obtained from other instruments, we need to convert our instrumental magnitudes into the magnitudes defined in the standard $UBVRI$ system. To perform this conversion, it is essential to know the transformation equations, which are usually expressed as:

$$u = U + Z_U + k'_U X + C_U(U - B)\,, \tag{3}$$

$$b = B + Z_B + k'_B X + C_B(B - V)\,, \tag{4}$$

$$v = V + Z_V + k'_V X + C_V(B - V)\,, \tag{5}$$

$$r = R + Z_R + k'_R X + C_R(V - R)\,, \tag{6}$$

$$i = I + Z_I + k'_I X + C_I(V - I)\,. \tag{7}$$

where $ubvri$ are the instrumental magnitudes, $UBVRI$ are the standard magnitudes, Z_U, Z_B, Z_V, Z_R, and Z_I are the zero point magnitudes, k'_U, k'_B, k'_V, k'_R, and k'_I are the first-order extinction coefficients, C_U, C_B, C_V, C_R, and C_I are the color terms, and X is the airmass. The above parameters can be simultaneously determined by observing a series of Landolt standard stars covering a certain range of airmass and color (Landolt 1992).

Observations of Landolt standard stars were conducted on 12 photometric nights, spanning the period from Oct. 2004 to Mar. 2012. Most of these photometric nights were moonless or crescent nights, with a steady, cloudless sky. For a better comparison of these observations obtained at different times, we divided the photometric nights and the corresponding results into three epochs: Epoch 1 (2004–2005), Epoch 2 (2006–2007), and Epoch 3 (2011–2012).

Table 3 lists part of Landolt standard stars that were observed during Epoch 3. The typical exposure time for these stars is 300 s in U, 60 s in B, 40 s in V, 20 s in R, and 20 s in I. The photometric data of these Landolt standard stars were reduced using the "apphot" package of IRAF. The deduced coefficients in the transformation Equations (3)–(7) are shown in Table 4.

The photometric data obtained at different epochs seem to give a similar mean value of the relevant coefficients except for the magnitude zero points. The large difference in the magnitude zero point between Epoch 3 and the other two epochs is primarily related to the specific definition of the magnitude zero point, e.g., with an offset of 5.0 mag in all of the $UBVRI$ bands. The mean atmospheric extinction coefficients[5] at Xinglong Observatory, obtained with the most recent data (e.g., Epoch 3), are 0.55$\pm$0.06 in U, 0.35$\pm$0.02 in B, 0.24$\pm$0.02 in V, 0.17$\pm$0.02 in R, and 0.09$\pm$0.02 in I. Recently, Zhou et al. (2009) also examined the atmospheric extinction at Xinglong based on the observations with the 85-cm telescope. Their studies show that the first-order atmospheric extinction coefficients in the BVRI bands are 0.33$\pm$0.01, 0.24$\pm$0.01, 0.20$\pm$0.01, and 0.07$\pm$0.01, respectively, which are consistent with ours within the quoted errors. In Table 5, we also compared our results with two earlier estimates for the site given by Shi et al. (1998).

The color terms determined at the above three epochs are generally in accordance with each other, except in the U band where the variation is likely related to the change of the CCD that directly determines the quantum efficiency and hence the profile of the instrumental response curve. The 1300B-1 CCD was used during the periods over Epoch 1 and Epoch 3, and the corresponding photometric system has a larger U-band color term; the 1300B-2 CCD photometric system has a smaller value.

Figure 3 shows the correlations between the Landolt colors (Landolt 1992) and the instrument colors of TNT transformed by Equations (3)–(7). The Landolt standard stars observed on 2011 Dec

[5] The extinction coefficients are in units of magnitude per airmass.

Table 3 Landolt Standard Stars Used for the Photometric Calibration in 2011 and 2012

Star	α (2000)	δ (2000)	V	$B-V$	$U-B$	$V-R$	$R-I$	$V-I$
92_263	00:55:40	+00:36:23	11.782	1.048	0.843	0.563	0.522	1.087
93_317	01:54:38	+00:43:11	11.546	0.488	−0.055	0.293	0.298	0.592
94_251	02:57:46	+00:16:18	11.204	1.219	1.281	0.659	0.587	1.247
95_190	03:53:13	+00:16:39	12.627	0.287	0.236	0.195	0.220	0.415
96_83	04:52:59	−00:14:22	11.719	0.179	0.202	0.093	0.097	0.190
97_75	05:57:55	−00:09:07	11.483	1.872	2.100	1.047	0.952	1.999
98_666	06:52:10	−00:23:12	12.732	0.164	−0.004	0.091	0.108	0.200
100_280	08:53:36	−00:36:24	11.799	0.494	−0.002	0.295	0.291	0.588
101_413	09:56:15	−00:11:44	12.583	0.983	0.716	0.529	0.497	1.025
103_626	11:56:47	−00:21:47	11.836	0.413	−0.057	0.262	0.274	0.535
104_598	12:45:17	−00:16:41	11.479	1.106	1.050	0.670	0.546	1.215
105_815	13:40:04	−00:02:19	11.453	0.385	−0.237	0.267	0.291	0.560
106_1024	14:40:07	+00:01:31	11.599	0.332	0.085	0.196	0.195	0.390
107_484	15:40:17	−00:21:31	11.311	1.237	1.291	0.664	0.577	1.240
108_475	16:37:00	−00:35:01	11.309	1.380	1.462	0.744	0.665	1.409
109_381	17:44:12	−00:20:55	11.730	0.704	0.225	0.428	0.435	0.861
110_280	18:43:07	−00:04:02	12.996	2.151	2.133	1.235	1.148	2.384
111_1965	19:37:42	+00:26:30	11.419	1.710	1.865	0.951	0.877	1.830
112_250	20:42:27	+00:07:25	12.095	0.532	−0.025	0.317	0.323	0.639
113_260	21:41:49	+00:23:39	12.406	0.514	0.069	0.308	0.298	0.606
114_750	22:41:45	+01:12:30	11.916	−0.041	−0.354	0.027	−0.015	0.011
RU_152E	07:27:25	−01:58:47	12.362	0.042	−0.086	0.030	0.034	0.065
PG1047+003C	10:50:18	−00:00:21	12.453	0.607	−0.019	0.378	0.358	0.737
PG2349+002	23:51:53	+00:28:17	13.277	−0.191	−0.921	−0.103	−0.116	−0.219

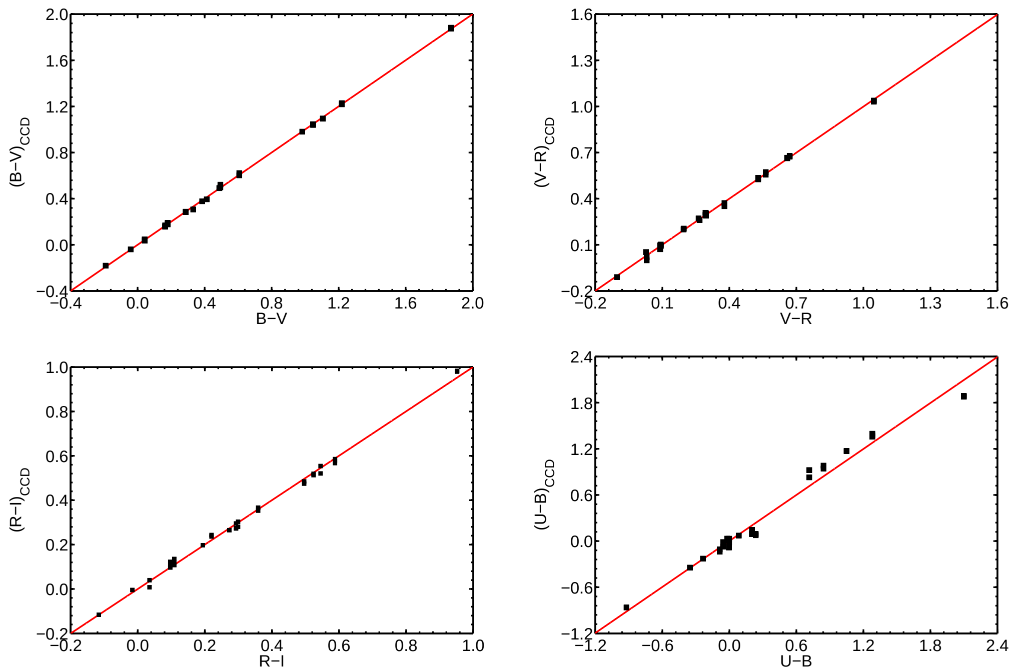

Fig. 3 The relationship between the Landolt (1992) color indices and the colors deduced from the transformation Eqs. (3)–(7). The data taken on 2011 Dec 31 are used for the plot.

Table 4 Transformation coefficients of zero-point magnitudes, first-order atmospheric extinction coefficients, and color terms in the $UBVRI$ bands, derived from the calibration data of 12 photometric nights.

Date (ymd)	Z_U	Z_B	Z_V	Z_R	Z_I
20041026	1.162±0.145	−1.317±0.046	−1.711±0.036	−1.671±0.039	−0.872±0.032
20041127		−1.356±0.028	−1.687±0.021	−1.604±0.020	−0.875±0.017
20050902		−1.023±0.017	−1.502±0.011	−1.552±0.016	−0.910±0.024
Epoch1 mean	1.162±0.048	−1.232±0.019	−1.633±0.014	−1.609±0.016	−0.886±0.014
20061221	−0.186±0.046	−1.854±0.024	−2.040±0.021	−2.155±0.020	−1.692±0.029
20070107	0.032±0.045	−1.798±0.034	−1.978±0.028	−2.113±0.026	−1.573±0.021
20070111	−0.042±0.061	−1.770±0.025	−1.935±0.020	−2.048±0.017	−1.586±0.024
20071212	−0.123±0.061	−1.837±0.032	−2.025±0.032	−2.085±0.033	−1.659±0.028
Epoch2 mean	−0.080±0.027	−1.815±0.014	−1.995±0.013	−2.100±0.012	−1.628±0.012
20111024	5.650±0.369	3.535±0.082	3.210±0.036	3.231±0.019	3.691±0.068
20111223	5.524±0.105	3.620±0.016	3.259±0.010	3.304±0.008	3.729±0.036
20111231	5.900±0.066	3.646±0.049	3.214±0.071	3.350±0.040	3.756±0.045
20120306		3.900±0.126	3.650±0.110	3.650±0.119	4.200±0.117
20120327		3.982±0.035	3.566±0.027	3.595±0.029	4.047±0.021
Epoch3 mean	5.691±0.078	3.737±0.033	3.380±0.028	3.426±0.026	3.885±0.030
Date (ymd)	k'_U	k'_B	k'_V	k'_R	k'_I
20041026	0.699±0.095	0.311±0.030	0.211±0.023	0.153±0.025	0.069±0.020
20041127		0.306±0.020	0.201±0.014	0.121±0.015	0.089±0.011
20050902		0.272±0.011	0.184±0.008	0.149±0.011	0.092±0.016
Epoch1 mean	0.699±0.032	0.296±0.012	0.199±0.009	0.141±0.010	0.083±0.009
20061221	0.648±0.027	0.295±0.014	0.201±0.012	0.152±0.011	0.099±0.016
20070107	0.548±0.028	0.295±0.020	0.214±0.016	0.175±0.015	0.074±0.012
20070111	0.644±0.040	0.332±0.016	0.220±0.013	0.158±0.011	0.093±0.016
20071212	0.709±0.038	0.307±0.020	0.221±0.020	0.158±0.021	0.097±0.018
Epoch2 mean	0.637±0.017	0.307±0.009	0.214±0.008	0.161±0.008	0.091±0.008
20111024	0.548±0.242	0.310±0.055	0.180±0.021	0.130±0.021	0.104±0.053
20111223	0.602±0.147	0.309±0.009	0.220±0.006	0.161±0.009	0.089±0.024
20111231	0.510±0.053	0.360±0.038	0.316±0.026	0.215±0.046	0.120±0.030
20120306		0.447±0.086	0.242±0.074	0.180±0.078	0.031±0.079
20120327		0.314±0.025	0.222±0.020	0.153±0.020	0.083±0.016
Epoch3 mean	0.553±0.058	0.348±0.022	0.236±0.017	0.168±0.019	0.085±0.021
Date(ymd)	C_U	C_B	C_V	C_R	C_I
20041026	−0.301±0.023	−0.190±0.011	0.077±0.009	0.135±0.017	−0.043±0.007
20041127		−0.165±0.005	0.083±0.004	0.146±0.006	−0.036±0.003
20050902		−0.229±0.005	0.067±0.004	0.085±0.009	−0.024±0.007
Epoch1 mean	−0.301±0.008	−0.195±0.004	0.076±0.003	0.122±0.007	−0.034±0.003
20061221	−0.132±0.016	−0.132±0.008	0.086±0.007	0.110±0.011	−0.037±0.009
20070107	−0.107±0.013	−0.128±0.011	0.076±0.009	0.106±0.016	−0.035±0.007
20070111	−0.136±0.011	−0.134±0.006	0.080±0.005	0.105±0.007	−0.040±0.005
20071212	−0.124±0.016	−0.133±0.007	0.079±0.007	0.101±0.013	−0.038±0.006
Epoch2 mean	−0.125±0.007	−0.132±0.004	0.080±0.004	0.106±0.006	−0.038±0.004
20111024	−0.316±0.063	−0.144±0.011	0.068±0.007	0.108±0.007	−0.026±0.011
20111223	−0.218±0.027	−0.149±0.002	0.064±0.004	0.095±0.004	−0.023±0.006
20111231	−0.367±0.034	−0.146±0.010	0.064±0.009	0.076±0.015	−0.025±0.007
20120306		−0.164±0.035	0.071±0.029	0.088±0.055	−0.015±0.031
20120327		−0.155±0.008	0.062±0.007	0.083±0.014	−0.033±0.005
Epoch3 mean	−0.300±0.015	−0.152±0.008	0.066±0.006	0.090±0.012	−0.024±0.007

Table 5 Atmospheric Extinction Coefficients at the Xinglong Observatory

Year	k'_B	k'_V	k'_R	k'_I	Reference
2011–2012	0.348±0.022	0.236±0.017	0.168±0.019	0.085±0.021	[1]
2008	0.330±0.007	0.242±0.005	0.195±0.004	0.066±0.003	[2]
2006–2007	0.307±0.009	0.214±0.008	0.161±0.008	0.091±0.008	[1]
2004–2005	0.296±0.012	0.199±0.009	0.141±0.010	0.083±0.009	[1]
1995	0.35	0.20	0.18	0.16	[3]
1989	0.31	0.22	0.14	0.10	[3]

References: [1] this paper; [2] Zhou et al. (2009); [3] Shi et al. (1998).

31 are used for the plot. Fitting those data points in a linear fashion yields a slope that is very close to 1.0, with an rms < 0.1 mag in different filters[6]. This means that the transformation from the photometric system of TNT to the Johnson-Cousins standard photometric system can be well established.

Note that the above color coefficients are obtained from normal stars with the $B - V$ color ranging from -0.3 mag to +2.2 mag, and may not account for all the photometric differences between the instrumental magnitudes and the standard Johnson-Cousins magnitudes for some variable sources such as SNe and GRBs because of their peculiar spectral shapes and features. Besides the color term correction, additional corrections such as the S-correction (Stritzinger et al. 2002) are usually required for precise photometry of these objects.

5 SYSTEM PERFORMANCE

5.1 System Efficiency

Using the photometric observations of Landolt standard stars, we could also estimate the total throughput of the overall observation system. This involves the filter response, the atmospheric transmission, the telescope optics and the detector quantum efficiency. Following the descriptions by Kinoshita et al. (2005) (see their eqs. (15)–(18)), we computed the throughput efficiency of the 1300B-1 CCD for the TNT observations. The results in different bands are summarized in Table 6, with higher throughput efficiency in the V and R bands. This is in accordance with the light curves describing the CCD quantum efficiency provided by the manufacturers.

Table 6 The total throughput of the TNT photometric system for the $UBVRI$ bands, including telescope optics, filter transmittance, and detector quantum efficiency.

Band	U	B	V	R	I
Throughput	9.5%	12.1%	24.7%	36.4%	13.6%

5.2 Sky Background Brightness

As a byproduct of our photometric calibrations, we could also estimate the brightness of the night sky based on the flux of the sky background. The instrumental magnitudes were converted into the standard system with the transformation Equations (3)–(7) and the coefficients shown in Table 3. We did not consider the effects caused by the difference in the airmass and the direction of the sky area[7]. As the sky background emission is affected significantly by the moon phase, we divided the

[6] The scatter in U is slightly larger ($\sim$0.58 mag) due to relatively lower quality data.

[7] Xinglong Observatory is located 115 km northeast of Beijing, 200 km northeast of Tianjin, and 7 km east of Xinglong county. The city lights from Beijing, Tianjin, and Xinglong can contribute significantly to the western sky background around the Xinglong Observatory.

Table 7 The background brightness of the night sky at the Xinglong Observing Station. The brightness is expressed in the unit of mag arcsec^{-2}.

Date (ymd)	U	B	V	R	I
20041026	19.831±0.261	19.434±0.079	19.211±0.060	18.961±0.441	18.321±0.180
20041127		19.377±0.044	19.467±0.032	19.226±0.186	18.672±0.081
20070107	19.388±0.186	19.725±0.050	19.678±0.042	19.471±0.393	18.650±0.155
20120306		17.025±0.015	16.857±0.015	16.525±0.019	16.212±0.018
moonlit above					
20050902		21.724±0.024	21.451±0.016	20.914±0.243	19.411±0.180
20061221	22.312±0.287	22.195±0.035	21.416±0.031	20.474±0.309	18.908±0.225
20070111	21.709±0.148	21.606±0.039	21.083±0.031	20.358±0.197	19.079±0.143
20071212	21.405±0.269	21.279±0.049	20.764±0.049	20.142±0.363	18.896±0.165
20111024	22.352±0.465	21.129±0.147	19.847±0.086	19.279±0.101	18.117±0.062
20111223	21.571±0.147	21.270±0.091	20.286±0.063	19.486±0.061	17.970±0.035
20111231	20.655±0.077	20.490±0.063	20.110±0.042	19.382±0.045	18.100±0.026
20120327		20.995±0.061	20.106±0.043	19.371±0.044	18.109±0.028
moonless above					
1989 10		22.15	21.04	20.25	18.77
1995 10		21.81	20.60	20.22	18.46

data from the 12 nights into two groups: moonlit and moonless nights. During the moonless nights (2004∼2007), the sky brightness was estimated to ∼21.8 mag in U, ∼21.7 mag in B, ∼21.2 mag in V, ∼20.5 mag in R, and ∼19.1 mag in I. These values are generally consistent with the estimates obtained in 1989 and 1995 (Shi et al. 1998, see also Table 7). The value of V is also consistent with the mean value of the moonlight-corrected sky brightness derived from the BATC data (Liu et al. 2003). In 2011, however, the sky brightness was found to be ∼21.3 mag in U, ∼20.9 mag in B, ∼20.0 mag in V, ∼19.3 mag in R, and ∼18.1 mag in I. These values are apparently brighter than those obtained a couple of years ago, indicating that the sky background at Xinglong Observatory has become worse in recent years. This is perhaps related to the contamination of the city lights of Beijing, Tianjin, and Xinglong.

5.3 Limiting Magnitude and Photometric Precision

We estimated the limiting magnitudes of the TNT photometric system as well. We used the equation below (Howell 2000) to perform our calculation

$$\frac{S}{N} = \frac{N_{\rm star}}{\sqrt{N_{\rm star} + n_{\rm pix}(N_{\rm sky} + N_{\rm dark} + N^2_{\rm readout})}}. \tag{8}$$

$N_{\rm star}$ is the total number of photons collected from the targets. $N_{\rm sky}$ is the total number of photons per pixel from the sky background. $N_{\rm dark}$ is the dark current per pixel from thermal electrons. $N_{\rm readout}$ is the readout noise estimated in Section 2.2. $n_{\rm pix}$ is the number of pixels under consideration for the calculation. The dark current electrons are neglected here.

The limiting magnitudes derived on the moonless nights with an aperture size of $6''$ in a slow readout mode are listed in Table 8, with mean values of $U \sim 19.2$ mag, $B \sim 19.0$ mag, $V \sim 18.8$ mag, $R \sim 18.7$ mag, and $I \sim 18.2$ mag, for a signal-to-noise ratio (SNR) of 100 and an integration time of 300 s. Compared with the detection limit for the 85-cm telescope obtained by Zhou et al. (2009, see their table D.2), TNT seems to go slightly deeper, e.g. 18.8 mag vs. 18.2 mag in V for a 300-s exposure, given a similar exposure time and SNR.

We further estimated the photometric precision of the TNT system. The errors of 1684 data points for the observations of 73 Landolt standard stars are shown in Figure 4. It is clearly seen that the photometric precision is ≤ 0.01 mag for sources brighter than 15.0 mag, with an exposure time

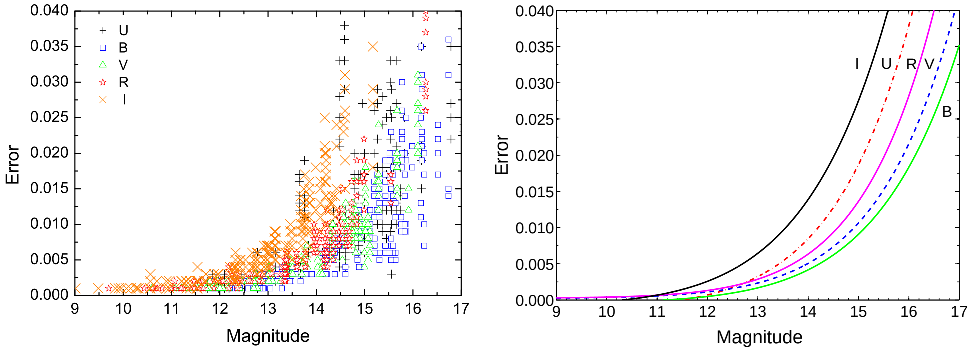

Fig. 4 Photometric errors of 73 Landolt standard stars obtained by the TNT system. Symbols in the left panel show the distribution of the observed values in the $UBVRI$ filters while the curves in the right panel represent the best fit to the corresponding data points.

Table 8 Limiting magnitudes (for an SNR of 100) derived in the slow mode using the data taken on moonlit and moonless nights with an exposure time of 300 s and a photometric aperture of $6''$.

Date (ymd)	U	B	V	R	I
20041026	18.280±0.122	18.091±0.038	17.984±0.029	17.863±0.215	17.551±0.089
20041127		18.064±0.021	18.107±0.015	17.992±0.090	17.723±0.039
20070107	18.069±0.089	18.230±0.024	18.207±0.020	18.109±0.189	17.712±0.076
20111006		17.795±0.021	17.666±0.021	17.889±0.020	17.936±0.021
20120306		17.577±0.007	17.527±0.007	17.744±0.009	17.785±0.009
moonlit mean	18.175±0.030	17.951±0.011	17.898±0.009	17.919±0.060	17.741±0.025
20050902		19.108±0.009	19.000±0.007	18.773±0.107	18.080±0.087
20061221	19.321±0.092	19.280±0.012	18.985±0.013	18.577±0.142	17.838±0.109
20070111	19.102±0.056	19.061±0.015	18.846±0.013	18.525±0.091	17.920±0.069
20071212	18.981±0.107	18.929±0.021	18.707±0.022	18.425±0.170	17.832±0.080
20111024	19.353±0.017	19.001±0.015	18.697±0.016	18.761±0.016	18.452±0.016
20111223	19.257±0.008	19.078±0.008	18.865±0.009	18.855±0.009	18.410±0.010
20111231	19.116±0.006	18.902±0.008	18.772±0.007	18.815±0.007	18.474±0.007
20120327		19.104±0.029	18.902±0.021	18.919±0.021	18.582±0.013
moonless mean	19.215±0.019	19.058±0.006	18.847±0.005	18.706±0.033	18.199±0.022

of 300–600 s in U, 60–120 s in B, 40–90 s in V, 20–60 s in R, and 20–40 s in I. This is similar to the precision reached by the 85-cm telescope for a similar exposure time and SNR (Zhou et al. 2009).

6 SUMMARY

In this article, we evaluate the performance of the VersArray: 1300B CCD photometric system mounted on the Tsinghua-NAOC 0.8-m telescope at the Xinglong Observing Station of NAOC. Results of the evaluation are summarized as follows:

(1) Typical CCD parameters such as bias, gain, readout noise, and dark current are derived for VersArray:1300B. These parameters, especially the bias and the readout noise, are related to the readout modes. Compared with the fast readout mode, the slow mode produces an apparently lower bias level and readout noise. Because of a very low working temperature, the dark current of the CCD detector is very low and can be ignored in the image reduction.

(2) Based on the observations of Landolt standard stars over a dozen photometric nights, we derived the transformation coefficients between the instrumental $ubvri$ magnitudes and the standard $UBVRI$ magnitudes: (i) the color terms used to normalize the photometry are relatively small for the $ubvri$ filters mounted on TNT, suggesting that the response curves are similar to those of the standard Johnson/Cousins (Bessel) system; (ii) the atmospheric extinction coefficients in $UBVRI$ bands are robustly determined for the Xinglong site with our extensive calibration data taken on the photometric nights.

(3) The limiting magnitudes are also obtained for TNT. With an exposure time of 300 s, it can detect a point source with $B \sim 19.0$ mag and $V \sim 18.8$ mag for an SNR$\sim$100.

(4) The emission of the sky background at the Xinglong Observatory was also examined with our extensive calibration data, which shows an apparent increase after 2005, e.g. from a level of $V \sim 21.4$ mag in 2005 to $V \sim 20.2$ mag in 2011. This change definitely brings a negative effect on the astronomical observations and research programs at the Xinglong Observing Station.

Acknowledgements We thank the anonymous referee for his/her comments that helped to improve this manuscript. The work here is supported by the National Natural Science Foundation of China (Grants Nos. 11073013 and 11178003), the Foundation of Tsinghua University (Grant No. 2011Z02170), and the Major State Basic Research Development Program (Grant No. 2009CB824800).

References

Bessell, M. S. 1990, PASP, 102, 1181
Fang, X.-S., Gu, S.-H., Hui, H.-K., et al. 2012, RAA (Research in Astronomy and Astrophysics), 12, 93
Fu, J. N., Zha, Q., Zhang, Y. P., et al. 2009, PASP, 121, 251
Howell, S. B. 2000, Handbook of CCD Astronomy (ISBN 0-521-64834-3), Cambridge University Press
Kinoshita, D., Chen, C.-W., Lin, H.-C., et al. 2005, ChJAA (Chin. J. Astron. Astrophys.), 5, 315
Landolt, A. U. 1992, AJ, 104, 340
Li, H.-L., Yang, Y.-G., Su, W., Wang, H.-J., & Wei, J.-Y. 2009, RAA (Research in Astronomy and Astrophysics), 9, 1035
Liu, Y., Zhou, X., Sun, W.-H., et al. 2003, PASP, 115, 495
Liu, H., Wang, J., Mao, Y., & Wei, J. 2010, ApJ, 715, L113
Shi, H., Qiao, Q., Hu, J., & Lin, Q. 1998, Acta Astrophysica Sinica, 18, 99
Stritzinger, M., Hamuy, M., Suntzeff, N. B., et al. 2002, AJ, 124, 2100
Wang, X., Li, W., Filippenko, A. V., et al. 2008, ApJ, 675, 626
Wang, X., Li, W., Filippenko, A. V., et al. 2009, ApJ, 697, 380
Wu, C., Qiu, Y. L., Deng, J. S., Hu, J. Y., & Zhao, Y. H. 2005, AJ, 130, 1640
Wu, C., Qiu, Y. L., Deng, J. S., Hu, J. Y., & Zhao, Y. H. 2006, A&A, 453, 895
Xin, L. P., Zheng, W. K., Wang, J., et al. 2010, MNRAS, 401, 2005
Xin, L.-P., Liang, E.-W., Wei, J.-Y., et al. 2011, MNRAS, 410, 27
Yan, H., Burstein, D., Fan, X., et al. 2000, PASP, 112, 691
Yan, J., Li, H., & Liu, Q. 2012, ApJ, 744, 37
Yang, Y.-G., Wei, J.-Y., Kreiner, J. M., & Li, H.-L. 2010, AJ, 139, 195
Zhai, M., & Wei, J. Y. 2012, A&A, 538, A125
Zhai, M., Zheng, W. K., & Wei, J. Y. 2011, A&A, 531, A90
Zhang, T., Wang, X., Li, W., et al. 2010, PASP, 122, 1
Zhang, T. M., et al. 2012, arXiv:1208.6078
Zhou, A.-Y., Jiang, X.-J., Zhang, Y.-P., & Wei, J.-Y. 2009, RAA (Research in Astronomy and Astrophysics), 9, 349